Experimental Study on Slowing-Down Mechanism of Locked-Mode-Like Instability in LHD[*]

Yuki TAKEMURA[1,2], Kiyomasa WATANABE[1], Tokihiko TOKUZAWA[1],
Satoru SAKAKIBARA[1,2], Yoshiro NARUSHIMA[1,2], Masaaki OKAMOTO[3],
Satoshi OHDACHI[1,2], Yasuhiro SUZUKI[1,2], Katsumi IDA[1,2], Mikiro YOSHINUMA[1,2],
Hayato TSUCHIYA[1], Ichihiro YAMADA[1] and LHD Experiment Group

[1]*National Institute for Fusion Science, National Institutes of Natural Sciences, Toki 509-5292, Japan*
[2]*SOKENDAI (the Graduate University for Advanced Studies), Toki 509-5292, Japan*
[3]*National Institute of Technology, Ishikawa College, Ishikawa 929-0342, Japan*

In order to clarify the mechanism responsible for slowing down the precursor of an instability in Large Helical Device (LHD), whose behavior is similar to the locked mode instability in tokamaks, the spatial structure of the precursor of the locked-mode-like instability, and the relationship between the rotation of the precursor and the $\mathbf{E} \times \mathbf{B}$ rotation were experimentally investigated. The precursor rotates together with the $\mathbf{E} \times \mathbf{B}$ rotation at the resonant surface, and the precursor rotation slows down because of a decrease of the $\mathbf{E} \times \mathbf{B}$ rotation. The multi-channel fluctuation measurement of the precursor suggests that the precursor has a magnetic island, which may be related to the decrease of the $\mathbf{E} \times \mathbf{B}$ rotation. In addition, the reason for the appearance of the precursor with a magnetic island is discussed. The precursor appears when a magnetic island grows initially without rotation but then shrinks and begins to rotate.

1. Introduction

MHD stabilities in Large Helical Device (LHD) depend upon the magnetic configuration. In the standard LHD configuration, core MHD modes are stabilized by a magnetic well, and edge MHD modes are stabilized by high magnetic shear. Therefore, the reactor-relevant beta value of 5% as the volume averaged beta value has been achieved [1]. In such high-beta discharges, low-order rotating modes are excited at rational surfaces in the edge plasma region where the pressure gradient that drives the instability is steep, while the modes have little effect on plasma confinement [2]. Early experimental studies of the onset condition and the parameter dependence of the modes suggest that the low-order rotating modes are resistive interchange instabilities [3, 4].

Conversely, in discharges with low magnetic shear over the entire plasma region because of high aspect ratio configurations and/or a finite toroidal plasma current, a non-rotating $m/n = 1/1$ mode appears that has a magnetic island. Here, m and n are the poloidal and the toroidal mode number, respectively. After the non-rotating mode is excited, the flat region in the pressure profile near the resonant surface expands and the core pressure rapidly

drops, resulting in serious degradation of plasma confinement [5, 6]. In some discharges with non-rotating modes, the rotating $m/n = 1/1$ mode appears as a precursor, and its frequency decreases before the non-rotating mode grows larger. Such instabilities are called locked-mode-like instabilities [7]. It is important to study the driving mechanisms for the locked-mode-like instability in order to clarify the effects of magnetic shear on plasma confinement through MHD instabilities. Studies of the driving mechanisms may also be useful in evaluating the confinement performance of devices with low magnetic shear configurations, such as Wendelstein 7–X [8], and to clarify the physical mechanism of the locked mode instability in tokamaks.

Previous work [7] has shown that the locked-mode-like instability typically behaves as follows. First, when the precursor is excited, its amplitude and frequency are stationary. Second, after the magnetic shear decreases due to increasing plasma current, the amplitude increases, whereas the frequency decreases. Third, when the frequency becomes almost zero, i.e., when the rotation of the precursor stops, a non-rotating mode that has a magnetic island rapidly grows. The phase at which the rotation of the precursor stops, and the location at which the amplitude of the non-rotating mode is maximum, depend upon the amplitude of the external resonant magnetic perturbation (RMP) [7]. If the external RMP has a large amplitude,

the O-point of the non-rotating mode is located near that of the $m/n = 1/1$ magnetic island produced by the external RMP. Conversely, if the external RMP has a small amplitude, the O-point of the non-rotating mode is located anywhere.

It is not yet clear what mechanism are responsible for slowing down the rotation of MHD instabilities in helical and tokamak devices. For the locked mode instability in tokamaks, before its magnetic island grows rapidly, the amplitude of the MHD mode that is a precursor of the locked mode instability increases, while the frequency decreases [9, 10]. This behavior is similar to that of the locked-mode-like instability in LHD. The locked mode instability is a major cause of disruptions in tokamaks and is one of the critical issues for future machines such as ITER [11, 12]. In tokamaks, it is believed that electro-magnetic torques occurs because of interactions between the external RMP like an error field and the rotating magnetic island caused by the instability. This torque is a strong candidate for the slowing-down mechanism [13]. In this model, a precursor with a magnetic island is key for slowing down the rotation. Therefore, for the locked-mode-like instability in LHD, it is important whether or not the precursor has a magnetic island. Note that the interchange mode, which is the most unstable mode in LHD, does not have a meaningful magnetic island, according to linear MHD theory [14]. Moreover, during the slowing-down of the precursor for the locked mode instability in tokamaks, the MHD modes rotate together with the plasma. However, during the braking of the precursor for the locked-mode-like instability in LHD, the relationship between the plasma flow and the rotation of the precursor is unclear.

In this paper, the radial profile of the plasma flow and the precursor of the locked-mode-like instability were experimentally investigated in order to clarify the physical mechanism responsible for slowing down the mode rotation, which is key for the growth of the non-rotating mode. This study is important because experimental results for the locked-mode-like instability in LHD may also be useful for understanding the locked mode instability of tokamaks.

This paper is organized as follows. In Sec. 2, the experimental setup for measuring the radial profile of the $\mathbf{E} \times \mathbf{B}$ rotation and the precursor is explained. In Sec. 3, the radial profile of the $m/n = 1/1$ electron temperature fluctuations, and the relationship between the precursor rotation frequency and the $\mathbf{E} \times \mathbf{B}$ rotation frequency, are shown. In Sec. 4, the reason why the precursor with a magnetic island appears is discussed, and the paper is summarized in Sec. 5.

2. Experimental Setup

The poloidal magnetic fluctuations associated with the precursor of the locked-mode-like instability was measured using toroidal (poloidal) arrays of magnetic probes

[15]. The slowly evolving radial magnetic fluctuation associated with the non-rotating mode was measured using two poloidal arrays of saddle-loop coils [15]. The radial structure of the plasma flow was measured using charge exchange spectroscopy (CXS). The evaluation method of the $\mathbf{E} \times \mathbf{B}$ rotation frequency from the carbon flow measured by the CXS is discussed in [16]. The CXS requires the vertical injection of a neutral beam (NB). The internal radial profile of the precursor was measured using a multi-channel electron cyclotron emission (ECE) measurement system. The ECE signal is proportional to the electron temperature in the optically thick plasmas in the present LHD experiments. The operational toroidal magnetic field B_t was set at -1.375 T in order to measure the ECE fluctuations near the rational surface of the precursor. This is because a measurable region of the ECE measurement system depends on the B_t. The radial structure of the electron pressure was measured using a Thomson scattering system. The precursor is typically observed in discharges with a volume-averaged beta value of 1% and a low line-averaged electron density of $\sim 1 \times 10^{19}$ m^{-3} in configurations with low magnetic shear. To achieve low magnetic shear, the magnetic configuration is set at a high aspect ratio, and the toroidal plasma current in the co-direction is driven by tangential neutral beam injection (NBI). Here, the toroidal current in co- (cntr-) direction leads to an increase (decrease) of the rotational transform. Ne gas is introduced at the beginning of the discharge to induce a high plasma current. The locked-mode-like instability is clearly observed when the intrinsic error field is canceled by the RMP coils. Therefore, the external RMP is applied to cancellation of the intrinsic error field. The reason why the locked-mode-like instabilities are clearly observed in the discharge without the intrinsic error field is still not clear.

3. Radial Profile of Plasma Rotation and Precursor during Slowing-down

Figure 1 shows the time evolution of the plasma parameters in a discharge where the locked-mode-like instability appears. Figures 1 (a)-(c) show the volume-averaged beta value, the line-averaged electron density, and the toroidal plasma current normalized by B_t, respectively. Here, a positive value in Fig. 1 (c) indicates the current in the co-direction. The solid lines in Figs. 1 (d) and (e) are the amplitude of the poloidal component of the $m/n = 1/1$ magnetic fluctuation and the frequency of that fluctuation. The filled circles in Fig. 1 (e) are the $\mathbf{E} \times \mathbf{B}$ rotation frequency at the $\iota/2\pi = 1$ rational surface. Figure 1 (f) shows the amplitude of the slowly evolving radial component of the $m/n = 1/1$ magnetic fluctuation. Figure 1 (g) is a contour plot showing the time evolution of the radial profile of the $\mathbf{E} \times \mathbf{B}$ rotation frequency. The blue (red) region is the $\mathbf{E} \times \mathbf{B}$ rotation frequency in the ion (electron) diamagnetic direction. The filled circles show the
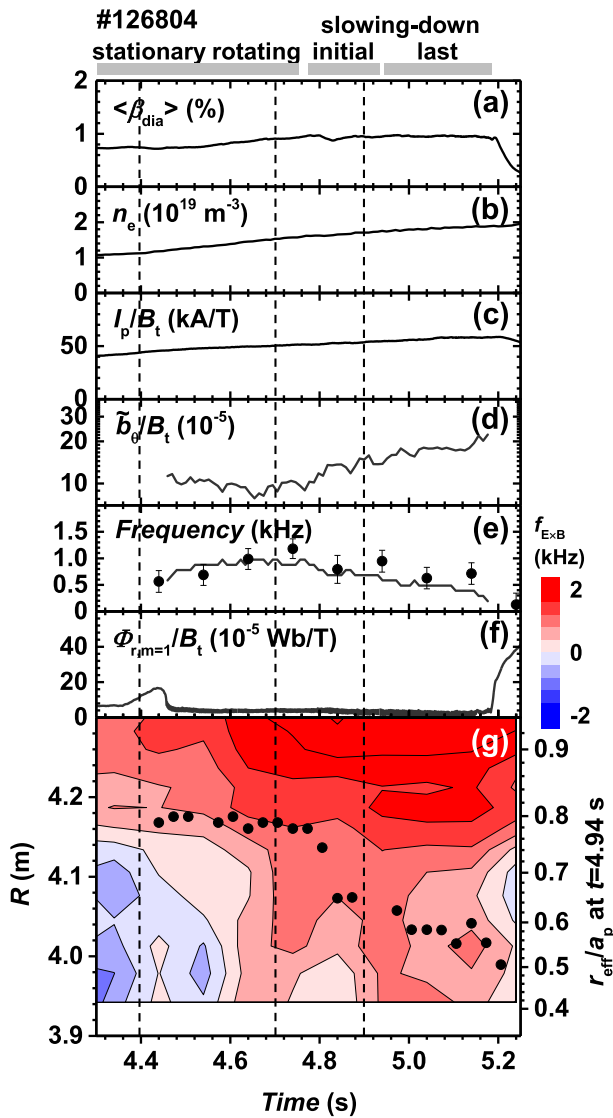
Fig. 1   Waveform of a typical discharge exhibiting the slowing-down phenomenon. (a) Volume-averaged beta value. (b) Line-averaged electron density. (c) Plasma current. (d) Amplitude of the poloidal component of the $m/n = 1/1$ magnetic fluctuation. (e) Frequency of the $m/n = 1/1$ magnetic fluctuation (solid line) and the $\mathbf{E} \times \mathbf{B}$ rotation frequency (filled circles with error bars). (f) Amplitude of the slowly evolving radial component of the magnetic fluctuation. (g) Contours of the radial profile of the $\mathbf{E} \times \mathbf{B}$ rotation frequency and the $\iota/2\pi = 1$ rational surface (filled circles). The three vertical dashed lines indicate the times corresponding to the radial profiles of the $m/n = 1/1$ mode shown in Fig. 3.

$\iota/2\pi = 1$ rational surfaces evaluated from the flattening region of the electron temperature profile. In this discharge, a plasma with a beta value of 1% and an electron density of $1 \sim 2 \times 10^{19}$ m^{-3} is produced and maintained by the tangential NBI (Figs. 1 (a) and (b)). The plasma current in the co-direction increases during the discharge (Fig. 1 (c)). The I_p/B_t value of ~ 50 kA corresponds to an increment of 10% from the edge rotational transform without the plasma cur-
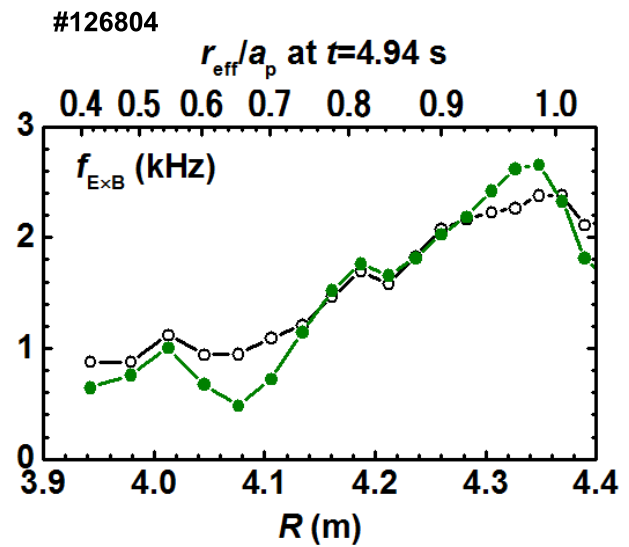
Fig. 2   The radial profile of the $\mathbf{E} \times \mathbf{B}$ rotation frequency at 4.94 s (open circles) in the first part of the slowing-down phase and at 5.14 s (filled circles) in the second part of the slowing-down phase. Open and filled arrows show the position of the rational surfaces at 4.94 s and 5.14 s, respectively.

rent. From Figs. 1 (d) and (e), the $m/n = 1/1$ mode rotating in the electron diamagnetic direction is excited. After excitation of the precursor, the amplitude and the frequency of the fluctuation are stationary. This is called the stationary rotating phase. After 4.76 s, the fluctuation amplitude grows, whereas the fluctuation frequency decreases. This is called the slowing-down phase. When the frequency is almost zero at 5.18 s, the non-rotating mode grows rapidly (Fig. 1 (f)).

     In order to clarify the relationship between the plasma flow and the fluctuation frequency in the slowing-down phase, the fluctuation frequency is compared with the $\mathbf{E} \times \mathbf{B}$ rotation frequency at the resonant surface. According to Fig. 1 (e), the both frequencies are almost the same. Therefore, the precursor rotates together with the plasma during the stationary rotating phase and during the slowing-down phase. From Fig. 1 (g), the decrease in the fluctuation frequency during the slowing-down phase is divided into two parts (4.76 ~ 4.94 s and 4.94 ~ 5.18 s). Figure 2 shows the radial profile of the $\mathbf{E} \times \mathbf{B}$ rotation frequency at the resonant surface at 4.94 and 5.14 s. The arrows in the figure correspond to the locations of the resonant surface. In the initial part of the slowing-down phase, the resonant surface moves toward the core region due to the increasing co-current. The $\mathbf{E} \times \mathbf{B}$ rotation frequency in the core region is smaller than that in the outer region as shown in Fig. 2. The $\mathbf{E} \times \mathbf{B}$ rotation frequency at the resonant surface decreases. In the last part of the slowing-down phase, the resonant surface does not move significantly. On the contrary, the $\mathbf{E} \times \mathbf{B}$ rotation frequency at the resonant surface decreases. Therefore, the movement
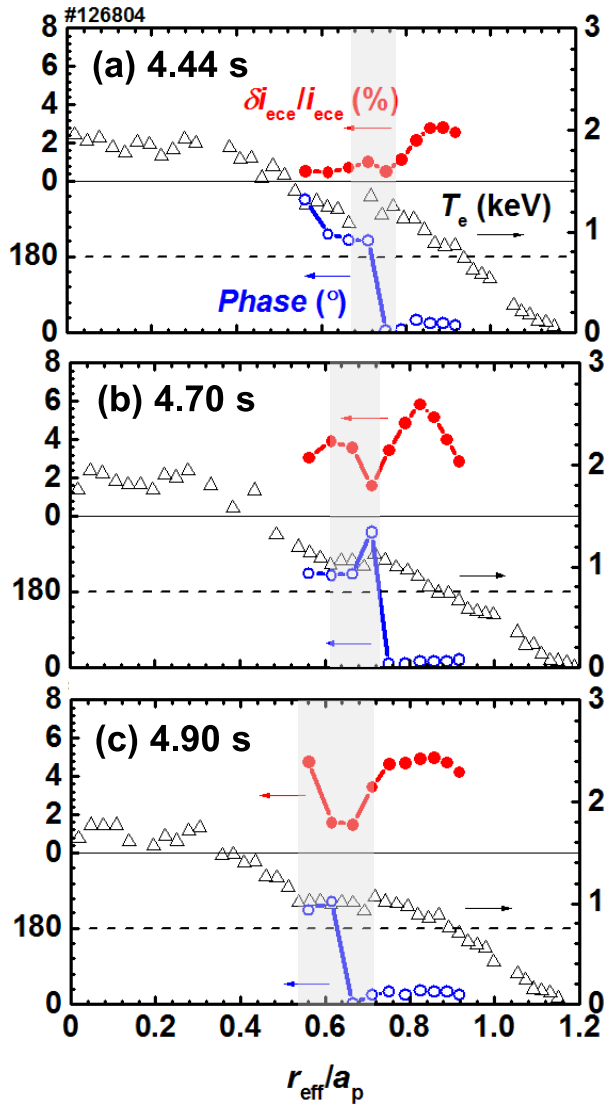
Fig. 3 Radial profiles of the $m/n = 1/1$ ECE fluctuations at 4.44, 4.70, and 4.90 s. Filled (open) circles show the amplitude (phase) of the ECE fluctuations. Open triangles show the electron temperature profile obtained from the Thomson scattering system. The gray shaded region denotes the flattening region in the electron temperature profile.

of the resonant surface plays an important role in the decrease of the fluctuation frequency in the initial part of the slowing-down phase, whereas the decrease of the $\mathbf{E} \times \mathbf{B}$ rotation frequency at the resonant surface plays an important role in the decrease of the fluctuation frequency during the last part.

In order to clarify whether or not the precursor has a magnetic island, the radial profile of the precursor was investigated. Figure 3 shows the radial profile of the $m/n = 1/1$ ECE fluctuations correlated with the precursor. Figures 3 (a) and (b) show the ECE fluctuation profile in the stationary rotating phase, while Fig. 3 (c) shows the profile in the slowing-down phase. The vertical lines in Fig. 1 indicate the times corresponding to Figs. 3 (a)-(c).

In these figures, the filled (open) circles are the amplitude (phase) of ECE fluctuations and the open triangles are the radial profiles of the electron temperature obtained from the Thomson scattering system. The grey shaded regions in these figures denote the flattening region of the electron temperature profile, which corresponds to the resonant surface. At 4.44 s, just after the precursor is excited, the radial structure of the amplitude of ECE fluctuations has two peaks near the resonant surface, and the phase difference between these peaks is almost inverted, as shown in Fig. 3 (a). Such structure is called an odd function structure. At 4.70 s in the stationary rotating phase and at 4.90 s in the slowing-down phase, the precursor with the odd function structure is also excited (Figs. 3 (b) and (c)). This behavior of the amplitude and the phase difference suggests that the precursor has a magnetic island. Note in case of resistive interchange instabilities, the radial structure of the amplitude has a peak near the resonant surface and the phase difference near the peak is almost same, i.e. an even function, according to the linear MHD theory.

It is noteworthy that the poloidal velocity of the plasma flow measured by microwave Doppler reflectometry is synchronized with the precursor, and that the velocity varies between zero and finite values. This result also suggests the existence of a rotating magnetic island [17].

4. Discussion of Precursor with Magnetic Island

In this section, the reason why the precursor with a magnetic island for the locked-mode-like instability in LHD is discussed. Figures 4 (a) and (b) show the time evolution of the poloidal and the radial components of the $m/n = 1/1$ magnetic fluctuation, respectively. Figures 4 (c) and (d) show the same information as Figs. 4 (a) and (b), respectively, except on an expanded timescale. The poloidal component grows rapidly at 4.46 s in Figs. 4 (a) and (b), which means the precursor is excited. Before the precursor appears, the radial component suddenly grows at 4.36 s, becomes the maximum value of 17×10^{-5} Wb/T at 4.44 s, and then decreases to 13×10^{-5} Wb/T. The radial component is synchronized with the poloidal component, as shown in Figs. 4 (c) and (d). These results suggest that the non-rotating mode grows suddenly and then reduces in amplitude before starting to rotate. The reduction in amplitude following the sudden growth of the non-rotating mode is thought to play key role in the appearance of the precursor with a magnetic island.

In order to investigate the reason why the non-rotating mode begins to rotate, a discharge with a precursor, in which the non-rotating mode starts to rotate, is compared with a discharge without a precursor, in which the non-rotating mode continues not to rotate. The experimental conditions in both discharges are almost the same. Figures 5 (a)-(f) show the port-through power of the tangential NB, the toroidal plasma current normalized by B_t,
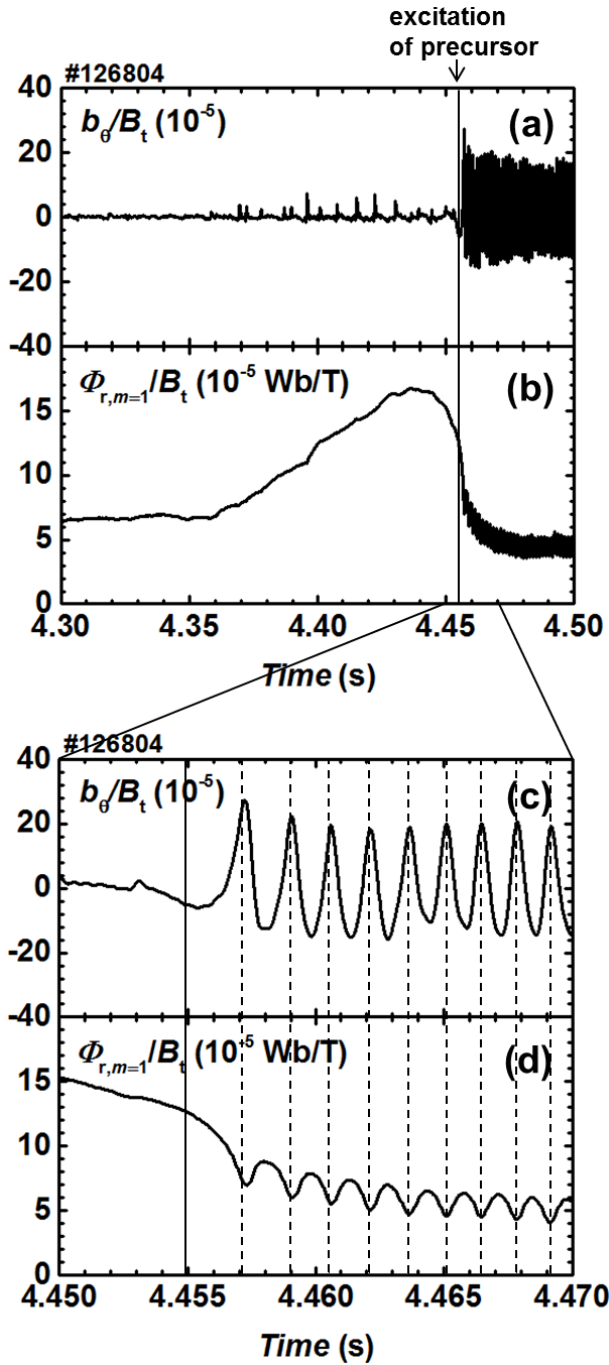
Fig. 4   (a) The poloidal component of the $m/n = 1/1$ magnetic fluctuation around the time when the precursor appears. (b) The slowly evolving radial component of the magnetic fluctuation. Panels (c) and (d) show the same information as panels (a) and (b), respectively, but on an expanded timescale. The vertical solid lines show the time when the precursor appears. The vertical dashed lines in Figs. 4 (c) and (d) correspond to the local maximum values of the poloidal component.

the volume-averaged beta value, the line-averaged electron density, the poloidal component of the $m/n = 1/1$ magnetic fluctuation measured by the magnetic probe, and the radial component of the $m/n = 1/1$ magnetic fluctuation
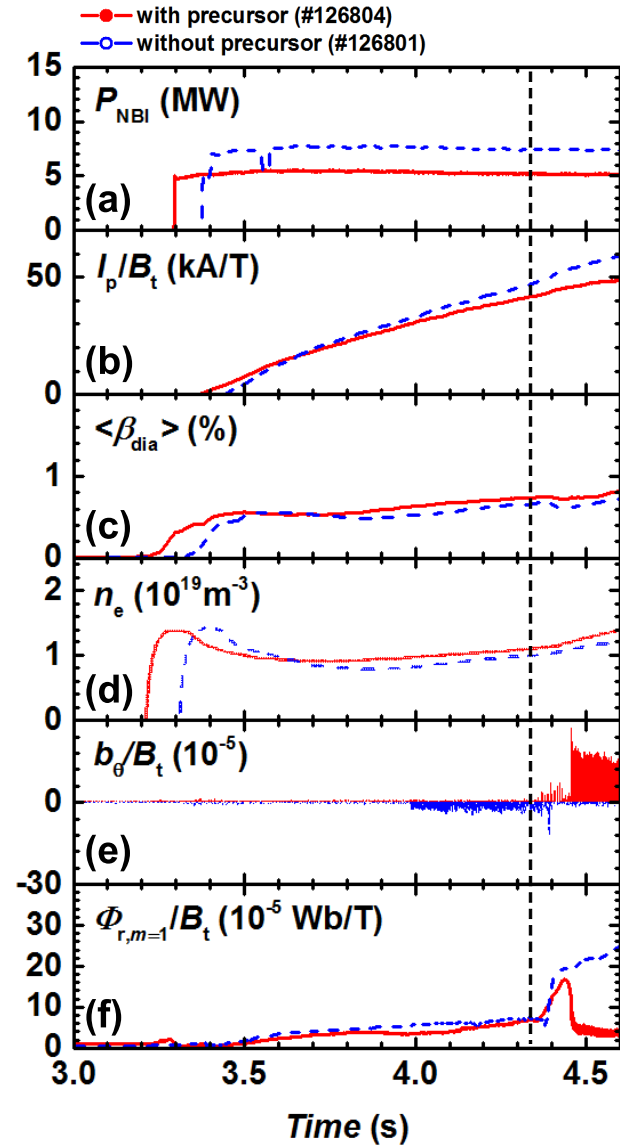
Fig. 5   Waveform in discharges with and without a precursor. (a) The port-through power of the tangential NBI. (b) The plasma current (positive current corresponds to an increase of the rotational transform). (c) The volume-averaged beta value. (d) The line-averaged electron density. (e) The poloidal component of the magnetic fluctuation (the upper half panel corresponds to the discharge with a precursor, while the lower half panel denotes the discharge without a precursor). (f) The amplitude of the slowly evolving radial component of the magnetic fluctuation. The vertical dashed line denotes the time corresponding to the radial profile shown in Fig. 6.

obtained using the saddle-loop coils, respectively. The amplitude of the non-rotating radial component of the magnetic fluctuation starts to increase at 4.36 s in both discharges, as shown in Fig. 5 (f). The amplitude decreases at 4.45 s in the discharge with a precursor. Conversely, the amplitude continues to increase in the discharge without a precursor. The plasma terminates at 4.68 s due to breakdown of the NBI in the discharge without a precursor. At
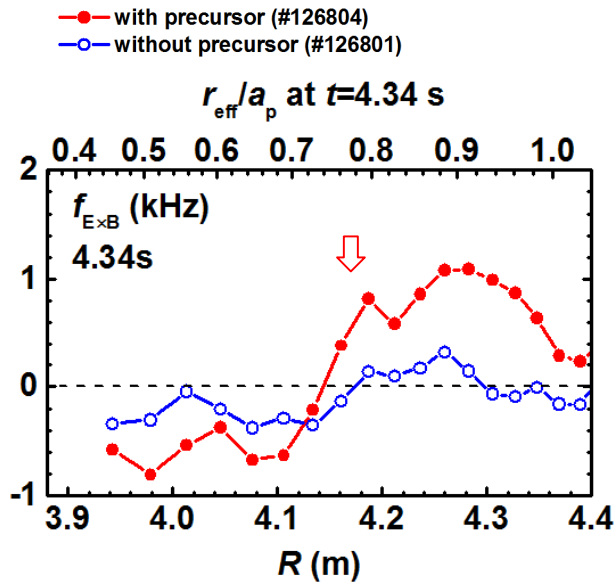
Fig. 6   The radial profiles of the $\mathbf{E} \times \mathbf{B}$ rotation frequency at 4.34 s in the discharges where the non-rotating mode does and does not start to rotate. The downward-pointing arrow shows the location of the rational surface.

Fig. 7   The $\mathbf{E} \times \mathbf{B}$ rotation frequency as a function of the radial magnetic fluctuation amplitude in the two types of discharges with and without a precursor. The filled circles denotes the $\mathbf{E} \times \mathbf{B}$ rotation frequency at the stage where the non-rotating mode starts to rotate in the discharge with a precursor. Crosses denote the $\mathbf{E} \times \mathbf{B}$ rotation frequency at 0.1 s after the start of growth of the non-rotating mode in the discharge without a precursor.

4.30 s, just before the amplitude of the radial component starts to grow, the port-through power of the tangential NB is slightly larger and the plasma current in the co-direction is also slightly higher in the discharge without a precursor, as shown in Figs. 5 (a) and (b). The volume-averaged beta value and the line-averaged electron density are almost the same, as shown in Figs. 5 (c) and (d). Figure 6 shows the radial profile of the $\mathbf{E} \times \mathbf{B}$ rotation frequency at 4.34 s just before the amplitude of the radial component starts to increase. The downward-pointing arrow indicates the position of the resonant surface in the discharge with a precursor. The $\mathbf{E} \times \mathbf{B}$ rotation frequency near the rational surface in the discharge with a precursor is higher than that in the discharge without a precursor. This suggests that the plasma flow affects the threshold at which the non-rotating mode begins to rotate.

Figure 7 shows the $\mathbf{E} \times \mathbf{B}$ rotation frequency at the rational surface as a function of the amplitude of the radial component of the $m/n = 1/1$ magnetic fluctuation in the two types of discharges. In the discharge with a precursor, the $\mathbf{E} \times \mathbf{B}$ rotation frequency is plotted at the point where the non-rotating mode starts to rotate. For the discharge without a precursor, the $\mathbf{E} \times \mathbf{B}$ rotation frequency is plotted at 0.1 s after the growth of the non-rotating mode begins. The $\mathbf{E} \times \mathbf{B}$ rotation frequency near the rational surface is almost zero in the discharge without the precursor, but it is higher than 0.3 kHz in the discharge with a precursor. For the discharges with a precursor, the radial magnetic fluctuation amplitude is larger in the discharge where the $\mathbf{E} \times \mathbf{B}$ rotation frequency is higher. It is worth noting that the radial magnetic fluctuation amplitude of $\sim 10 \times 10^{-5}$ Wb/T

corresponds to the magnetic island width normalized by the minor radius of 5%.

5. Summary

The aim of this paper is to clarify the slowing-down mechanism of the precursor of the locked-mode-like instability observed in low magnetic shear plasmas in LHD. The internal structure of the precursor and the relationship between the precursor rotation and the $\mathbf{E} \times \mathbf{B}$ rotation were experimentally investigated.

A comparison between the precursor rotation and the $\mathbf{E} \times \mathbf{B}$ rotation shows that the precursor rotates together with the $\mathbf{E} \times \mathbf{B}$ rotation at the resonant surface during the slowing-down of the precursor. The decrease of the $\mathbf{E} \times \mathbf{B}$ rotation at the resonant surface occurs as follows. First, the resonant surface moves into a region with slower $\mathbf{E} \times \mathbf{B}$ rotation. Second, the $\mathbf{E} \times \mathbf{B}$ rotation itself decreases near the resonant surface. Observations of the radial profile of the electron temperature fluctuation show that the precursor does have a magnetic island, which is known to be related to the slowing-down of the precursor to the locked mode instability in tokamaks. The slowing-down mechanism of the precursor to the locked-mode-like instability in LHD may contribute to the interaction between the rotating magnetic island and the RMP like an error field as may also be the case for the locked mode instability in tokamaks.

In addition, the reason why the precursor has a magnetic island was discussed. A comparison between discharges with and without a precursor to the locked-mode-like instability suggests that the precursor appears only if

the magnetic island starts to shrink and rotate after the non-rotating mode grows suddenly. The onset of rotation of the non-rotating mode requires a relatively large $\mathbf{E} \times \mathbf{B}$ rotation near the resonant surface.

For the locked-mode-like insatiability in LHD, it is not yet clear why the $\mathbf{E} \times \mathbf{B}$ rotation is significantly reduced in the last part of the slowing-down phase. For the locked mode instability in tokamaks, the decrease of plasma rotation is believed to be caused by the electromagnetic torque exerted by the magnetic island during the entire slowing-down phase. For the locked-mode-like instability, the precursor has a magnetic island which would expect also to exert the electro-magnetic torque during the whole slowing-down phase. However, no apparent reduction of the $\mathbf{E} \times \mathbf{B}$ rotation was observed in the beginning of the slowing-down phase. In order to understand the braking mechanism of the precursor to the locked-mode-like instability more thoroughly, the electro-magnetic torque during the whole slowing-down phase will be investigated in future work.

Acknowledgments

[1] A. Komori *et al.*, Nucl. Fusion **49**, 104015 (2009).
[2] K.Y. Watanabe *et al.*, Phy. Plasma **18**, 056119 (2011).
[3] S. Sakakibara *et al.*, Plasma Fusion Res. **1**, 049 (2006).
[4] S. Sakakibara *et al.*, Plasma Phys. Control. Fusion **50**, 124014 (2008).
[5] S. Sakakibara *et al.*, Fusion Sci. Technol. **50**, 177 (2006).
[6] S. Sakakibara *et al.*, Fusion Sci. Technol. **58**, 176 (2010).
[7] Y. Takemura *et al.*, Nucl. Fusion **52**, 102001 (2012).
[8] C. Nührenberg, Phys. Plasmas **3**, 2401 (1996).
[9] J.A. Snipes *et al.*, Nucl. Fusion **28**, 1085 (1988).
[10] J.T. Scoville *et al.*, Nucl. Fusion **31**, 875 (1991).
[11] T.C. Hender *et al.*, Progress in the ITER Physics Basis Chapter 3: MHD stability, operational limits and disruptions, Nucl. Fusion **47**, S128–202 (2007).
[12] R.J. Buttery *et al.*, Nucl. Fusion **39**, 1827 (1999).
[13] R. Fitzpatrick, Phys. Plasmas **1**, 3308 (1994).
[14] R. Ueda *et al.*, Phys. Plasmas **21**, 052502 (2014).
[15] S. Sakakibara, H. Yamada and LHD Experiment Group, Fusion Sci. Technol. **58**, 471 (2010).
[16] Y. Takemura *et al.*, Plasma Fusion Res. **8**, 1402123 (2013).
[17] T. Tokuzawa *et al.*, Magnetic island formation in locked-like mode in helical plasmas, The 26th IAEA Fusion Energy Conference (Kyoto, Japan, 2016).